HAL
open science

Influence of bulky groups in single-component conductors based on neutral radical gold bis(dithiolene) complexes

Hadi Hachem, Olivier Jeannin, Marc Fourmigué, Dominique Lorcy

To cite this version:

Hadi Hachem, Olivier Jeannin, Marc Fourmigué, Dominique Lorcy. Influence of bulky groups in single-component conductors based on neutral radical gold bis(dithiolene) complexes. Transition Metal Chemistry, 2023, 10.1007/s11243-023-00526-x . hal-04087910

HAL Id: hal-04087910

https://hal.science/hal-04087910v1

Submitted on 9 May 2023

HAL is a multi-disciplinary open access archive for the deposit and dissemination of scientific research documents, whether they are published or not. The documents may come from teaching and research institutions in France or abroad, or from public or private research centers.

L'archive ouverte pluridisciplinaire **HAL**, est destinée au dépôt et à la diffusion de documents scientifiques de niveau recherche, publiés ou non, émanant des établissements d'enseignement et de recherche français ou étrangers, des laboratoires publics ou privés.

Influence of bulky groups in single-component conductors based on neutral radical gold bis(dithiolene) complexes

Hadi Hachem, Olivier Jeannin, Marc Fourmigué, Dominique Lorcy*

Univ Rennes, CNRS, ISCR (Institut des Sciences Chimiques de Rennes) - UMR 6226, F-35000 Rennes, France

ORCID

Dominique Lorcy: 0000-0002-7698-8452

Marc Fourmigué: 0000-0002-3796-4802

Abstract

A novel single component conductor derived from neutral radical gold bis(dithiolene) complexes is prepared based on the original reactivity of *t*BuN-substituted 1,3-thiazoline-2-thione heterocycle to give a *t*BuS-substituted thiazole ring. The corresponding 2-(*tert*-butylthio)-1,3-thiazole-4,5-dithiolate ligand (*t*BuS-tzdt) forms the d^8 anionic complex $[Au(tBuS\text{-}tzdt)_2]^-$, easily oxidized through electrocrystallization into the neutral radical $[Au(tBuS\text{-}tzdt)_2]^\bullet$. The effect of increasingly bulky R groups (R = Et, $HO(CH_2)_2$, *t*Bu), in the series of such radical complexes $[Au(RS\text{-}tzdt)_2]^\bullet$, is investigated, with a focus on their solid state organization, either into face-to-face dimers or into non-dimerized, uniform stacks.

Keywords

Au complexes, dithiolene ligand, redox behavior, spectroelectrochemistry, conducting materials

Introduction

Over the last two decades, metal bis(dithiolene) complexes have demonstrated their great potential as precursors of Single-Component Molecular Conductors [1-4]. Within this family, two types of neutral complexes can be distinguished, (i) closed-shell complexes such as the neutral Ni bis(dithiolene) complexes abbreviated as $[Ni(dt)_2]^0$,[5-8] and (ii) open-shell

complexes based on gold bis(dithiolene) complexes in their radical neutral form, $[Au(dt)_2]^{\bullet}$.[9-15] In the gold series, we demonstrated that, when using a N-alkyl-1,3-thiazoline-2-thione-4,5-dithiolate ligand, the corresponding complexes $[Au(R\text{-thiazdt})_2]^{\bullet}$ (R = Et,[16-17] EtOH,[18] iPr,[19] Pr,[20]) exhibit high conductivities, becoming metallic under pressure while metallic at ambient pressure for the smallest substituent (R = Me) [21].

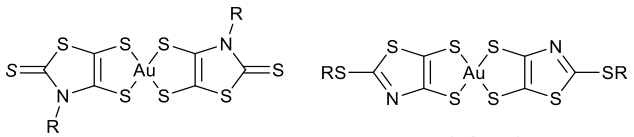

[**Au**(R-thiazdt)$_2$]
R = Me, Et, Pr, iPr, HO(CH$_2$)$_2$

[**Au**(RS-tzdt)$_2$]
R = Me, Et
R = tBu : this work

Interestingly, the presence of relatively bulky substituents on the thiazoline ring in $[Au(R\text{-thiazdt})_2]^{\bullet}$ complexes still allowed the neutral radical complexes to form uniform stacks in the solid state, with overlap patterns favorable for strong intermolecular overlap interactions and associated high conductivities [18-20]. In the course of our work on such gold bis(dithiolene) complexes, we also investigated another dithiolene ligand having a 2-alkylthio-1,3-thiazole backbone, to provide the corresponding neutral radical gold complexes $[Au(RS\text{-tzdt})_2]^{\bullet}$. They can be considered as the S-isomers of the $[Au(R\text{-thiazdt})_2]^{\bullet}$ complexes, but with now an aromatic thiazole ring [22-24]. With this idea in mind, we explored first the R = Me and R = Et substituents but both gold complexes, namely $[Au(MeS\text{-tzdt})_2]^{\bullet}$ and $[Au(EtS\text{-tzdt})_2]^{\bullet}$, form in the solid state strongly dimerized stacks with associated pairing of the radical species into diamagnetic dimers and the associated low conductivity. On the other hand, the introduction of a bulkier hydroxyethyl substituent allowed the organization of $[Au(HO(CH_2)_2S\text{-tzdt})_2]^{\bullet}$ into uniform stacks thanks to hydrogen bonding (HB) inter-stack interactions [23], between the OH group as HB donor and the nitrogen atom of the thiazole ring as HB acceptor. In the following, we want to investigate another stronger structural change in this tzdt series, which relies on the use of an even bulkier substituent such as a *tert*-butyl group in the corresponding $[Au(t\text{BuS-tzdt})_2]^{-1,\bullet}$ complexes. We report here on the preparation of the anionic and neutral gold complexes, and describe and analyze their electronic and structural properties.

Results and discussion

The synthesis of the anionic complex $[Au(tBuS\text{-tzdt})_2]^{-1}$ was performed according to the chemical route described in Scheme 1, starting from the N-*t*Bu-1,3-thiazoline-2-thione

proligand **1**. We used a chemical transformation of N-*tert*-butyl-1,3-thiazoline-2-thione heterocycles into 2-alkylthio-1,3-thiazole derivatives that we recently evidenced [22]. The synthesis of 2-(*tert*-butylthio)-1,3-thiazole-4,5-dithiolene proligand **2** involves therefore the reaction of **1** in CH_2Cl_2 in the presence of an excess of I_2. It is worth mentioning that when the reaction was performed in DMSO as previously described, we obtained instead the 2-iodothiazole proligand [24]. Using dichloromethane rather than DMSO, no trace of the 2-iodothiazole proligand was detected. Deprotection of the proligand **2** in the presence of sodium methanolate, followed by the addition of $KAuCl_4$ and PPh_4Br leads to the formation of the monoanionic gold complex as tetraphenylphosphonium salt, $[Ph_4P][Au(tBuS\text{-}tzdt)_2]$. Recrystallization from CH_3CN afforded crystals amenable to X-ray diffraction (*vide infra*). The monoanionic complex was oxidized electrochemically *via* electrocrystallization, in order to generate the corresponding neutral radical complex $[Au(tBuS\text{-}tzdt)_2]^{\bullet}$. Crystals of good quality of the neutral species were collected at the anode and also structurally characterized (*vide infra*).

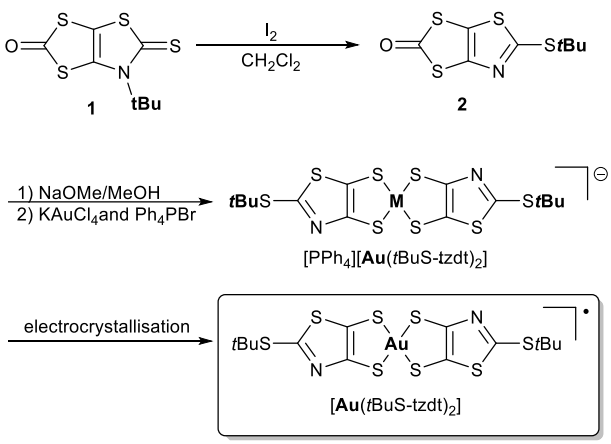

Scheme 1 Synthetic route toward neutral gold bisdithiolene complex $[Au(tBuS\text{-}tzdt)_2]^{\bullet}$

The redox properties of the anionic complex $[PPh_4][Au(tBuS\text{-}thiazdt)_2]$ were studied by cyclic voltammetry (CV) and the redox potentials are collected in Table 1 together with those of reference complexes with other 2-alkylthio substituents. The CV exhibits two well reversible oxidation waves corresponding to the successive oxidation of the monoanionic complex to the neutral radical species and then to the monocationic state. The shape of this voltammogram stands out from all other CV obtained so far for gold complexes with a thiazole backbone. Indeed, for all the other gold complexes with the RS-tzdt (R = Me, Et [22], $(CH_2)_2OH$ [23]) or R'-tzdt (R' = I, H) [24] ligands, only one pseudo reversible system was observed upon oxidation, with a sharp cathodic peak of higher intensity than the anodic peak, a consequence

of electrodeposition upon oxidation, followed on the reverse scan by a sharp desorption reduction peak. The fully reversible CV observed here for [PPh_4][Au(*t*BuS-tzdt)$_2$)] is due to a higher solubility of the neutral species generated upon oxidation, explaining the lack of adsorption phenomena (Fig. 1). As previously noted, the gold complex isomer with a N substituted ligand, *t*Bu-thiazdt [25], exhibits also upon anodic scan two reversible oxidation waves assigned similarly to the oxidation of the monoanionic complex into the neutral radical one and then to the monocationic complex. The main difference between these two CVs, and not the least, concerns the potential difference between these two redox processes. The presence of the aromatic thiazole backbone in [PPh_4][Au(*t*BuS-tzdt)$_2$)] induces a larger potential difference (ΔE = 460 mV) between the two redox processes, demonstrating the larger stability window of the radical species for the S-substituted ones, and a larger Coulombic repulsion *U*. This could be assigned to the structure of the dithiolene ligand backbone, which is aromatic in the case of tzdt ligand and non-aromatic for thiazdt one. Indeed, the oxidation of the gold bis(dithiolene) complexes essentially affects the AuS_2C_2 metallacycles, inducing some bond length modifications, with a shortening of the C−S bonds and a lengthening of the C=C bond. Both would induce for the tzdt ligand a loss of aromaticity. On the cathodic scan, as for all gold complexes of this family regardless of the substitution pattern of the ligand, an irreversible reduction process is observed for [PPh_4][Au(*t*BuS-tzdt)$_2$)], which corresponds to a metal-centered reduction of the monoanion to the dianionic species $E_{pc}^{(-1/-2)}$.

Table 1 Redox potentials in V *vs* SCE of gold bis(dithiolene) complexes.

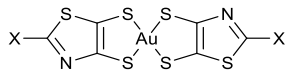

[**Au**(*X*-tzdt)$_2$]

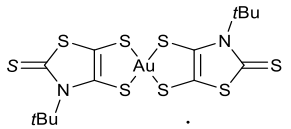

[**Au**(*t*Bu-thiazdt)$_2$]

	$E_{pc}^{(-1/-2)}$	$E_{pa}/E_{pc}^{(-1/0)}$	$E_{pa}/E_{pc}^{(0/+1)}$	Ref.
[PPh_4][Au(*t*BuS-tzdt)$_2$]	−1.18	+0.58/+0.52	+1.05/+0.98	this work
[PPh_4][Au(*t*Bu-thiazdt)$_2$]	−1.08	+0.49/+0.43	+ 0.57/-	25
[NBu_4][Au(I-tzdt)$_2$]	−1.05	+0.65/+0.46	-	24
[NBu_4][Au(H-tzdt)$_2$]	−1.19	+0.60/+0.43	-	24
[PPh_4][Au(HO(CH_2)$_2$S-tzdt)$_2$]	−1.12	+0.45/+0.28	-	23
[PPh_4][Au(EtS-tzdt)$_2$]	−1.04	+0.48/+0.44	-	22

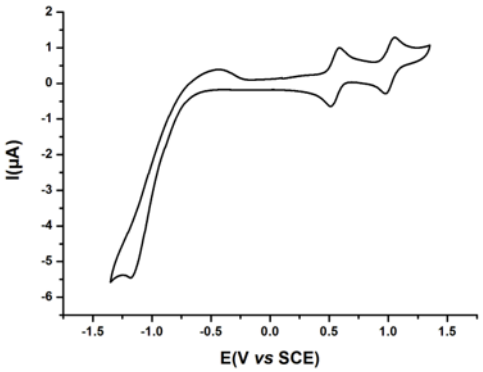

Fig. 1 Cyclic voltammogram of $[PPh_4][Au(tBuS\text{-}tzdt)_2)]$, in CH_2Cl_2 with NBu_4PF_6 as a supporting electrolyte, at 100 $mV.s^{-1}$

Spectroelectrochemical investigations

The higher solubility of $[Au(tBuS\text{-}tzdt)_2]^{\bullet}$ prompted us to realize a spectroelectrochemical investigation in order to determine the UV-Vis-NIR spectral signature of the different oxidation states of the gold complex. In its monoanionic state, the d^8 gold complex exhibits absorption bands limited to the UV-Vis region. Once the complex is oxidized to the neutral radical species, a broad band appears at 1614 nm, with a clear isosbestic point at 354 nm (Fig. 2). Further oxidation towards the monocation leads to the decrease of the 1614 nm absorption band, and the increase of a new absorption band centered at 1038 nm. Spectra of this cationic, high oxidation state are rare for gold bis(dithiolene) complexes, and have only been reported before by Wieghardt et *al*. for complexes with (*tert*-butylphenyl)$_2C_2S_2$ dithiolate ligands [26]. This evolution of the spectrum from the monoanionic to the monocationic state for gold complexes, parallels that oberved from the dianionic to the neutral state for the Ni, Pd, and Pt complexes. Furthermore, the absorption bands of the neutral gold complex are considerably red shifted when compared to the Ni complexes with the same ligands, as already mentionned with the gold and palladium bis(dithiolene) complexes of (*tert*-butylphenyl)$_2C_2S_2$ dithiolate ligand [26].

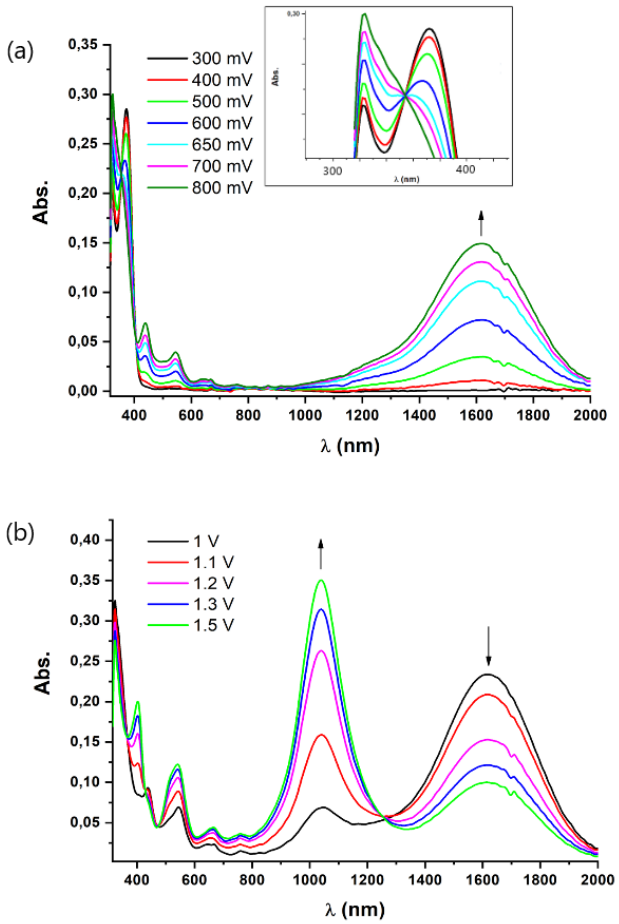

Fig. 2 UV-Vis-NIR absorption spectra of the electrochemical oxidation of $[PPh_4][Au(tBuS\text{-}tzdt)_2]$, (a) monitoring from 0.3V to 0.8 V (in insert the absorption between 300 and 400 nm with the isosbestic point showing at 354 nm), (b) monitoring from 1 V to 1.5 V.

Molecular structures

Both the monoanionic and the neutral crystalline complexes were investigated by single crystal X-ray diffraction. The molecular structures of the complex in both oxidation states are reported in Fig. 3. The monoanionic complex, $[PPh_4][Au(tBuS\text{-}tzdt)_2]$ crystallizes in the triclinic system, space group $P\bar{1}$, with a Ph_4P^+ cation and a gold complex located in general position in the unit cell. As shown in Fig. 3a, the complex is affected by disorder on both sides. In one side, the *t*Bu group exhibits a rotational disorder. On the other side, the disorder model indicates

unambiguously the presence of a *cis*-*trans* mixture, with 29% *trans* isomer (based on S5B, S6B) and 71% *cis* isomer (based on S5A, S6A).

The neutral radical complex, [Au(*t*BuS-tzdt)$_2$] crystallizes in the triclinic system, space group $P\bar{1}$, with the gold atom now located on an inversion center (Fig. 3b), with only the *trans* isomer. The *t*Bu moiety is disordered on two positions with almost 50:50 distribution, one where the S—CMe$_3$ bond is in the molecular plane with a 51% occupancy, and the other with the S—CMe$_3$ bond out of the molecular plane, rotated by 42°. Upon oxidation, a planarization of the metallacycles is observed with smaller dihedral angles along the S•••S hinge, from 3.66° in the monoanion to 1.98° in the neutral complex. Comparison of the bond distances between the monoanionic and neutral states (Table 2) shows a behavior similar to that observed in other gold bis(dithiolene) complexes, which is to say upon oxidation, the C−S bonds of the metallacycle (b, b') shorten and the C=C bonds (c) lengthen. Those changes in the bond lengths indicate the evolution of the 1,2-dithiolate ligand upon oxidation toward a more 1,2-dithioketone structure. Note also some modifications occurring on the thiazole ring: besides the lengthening of the C=C bond, the most significant ones are the lengthening of the C=N (g) bond and the shortening of the C−S (e) one (Table 2), demonstrating that the aromatic thiazole ring is also affected by the oxidation.

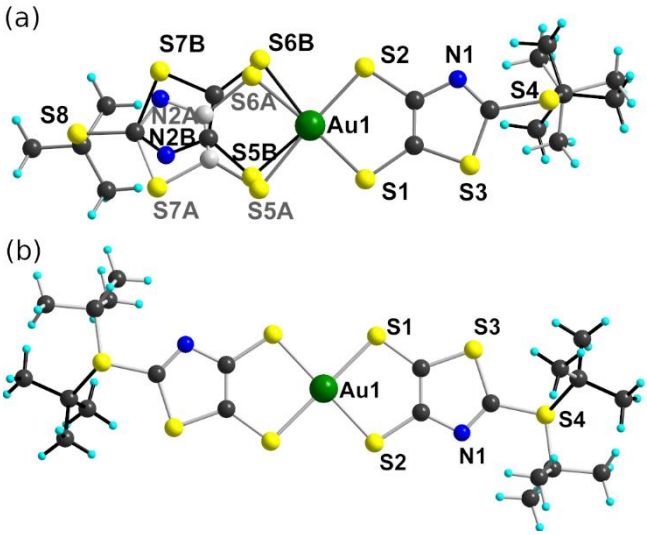

Fig. 3 Molecular views of (a) the anionic [Au(tBuS-tzdt)$_2$]$^-$ and, (b) the neutral radical [Au(tBuS-tzdt)$_2$]$^\bullet$ species. The disordered fragments are highlighted with black and light grey bonds (See text).

Table 2 Comparison of bond distances (Å) of the monoanionic and neutral complex

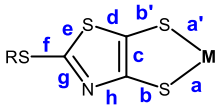

	a	a'	b	b'	c
$[Au(tBuS\text{-}tzdt)_2]^{-1}$	2.362(8)	2.286(6)	1.752(17)	1.797(17)	1.32(2)
$[Au(tBuS\text{-}tzdt)_2]^{\bullet}$	2.3174(13)	2.3082(15)	1.704(5)	1.729(5)	1.370(7)
	d	e	f	g	h
$[Au(tBuS\text{-}tzdt)_2]^{-1}$	1.742(14)	1.810(15)	1.752(13)	1.224(19)	1.42(2)
$[Au(tBuS\text{-}tzdt)_2]^{\bullet}$	1.729(5)	1.749(6)	1.740(5)	1.285(7)	1.417(7)

In the solid state, the radical complexes are not associated into dimers but form uniform stacks along the *a* axis, interacting sideways within *ab* layers (Fig. 4). Short S•••S contacts are evidenced between neighboring stacks, with the shortest contact at 3.505 Å involving sulfur atoms of the metallacycles. Within the stacks, a pronounced longitudinal slip is observed between the neighboring complexes with a plane-to-plane distance of 3.69 Å (Fig. 5).

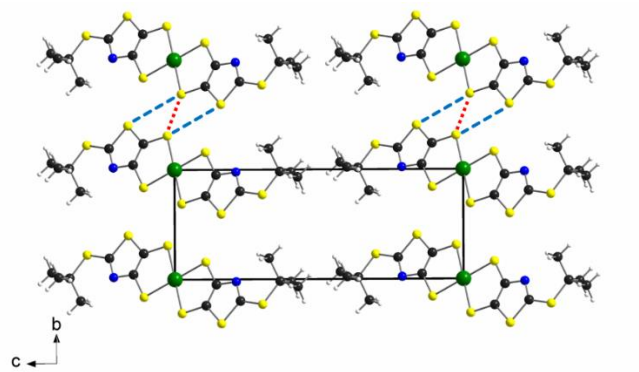

Fig. 4 Projection view along *a* of the unit cell of $[Au(tBuS\text{-}tzdt)_2]^{\bullet}$ with the shortest S•••S contacts indicated (dashed line, red : 3.505 Å and blue : 3.67 Å). Only the in-plane orientation of the *t*Bu group is shown.

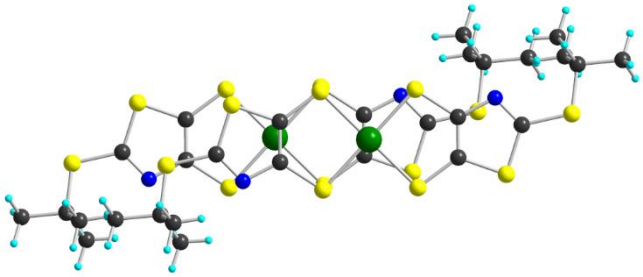

Fig. 5 Overlap pattern between neighboring molecules in the neutral radical complex [Au(*t*BuS-tzdt)$_2$]$^{\bullet}$. Only the in-plane orientation of the *t*Bu group is shown.

This overlap pattern is different than the one observed for the previously studied gold complexes with a 2-alkylthio thiazole backbone. For the other complex which also formed uniform stacks, [Au(HO(CH$_2$)$_2$S-tzdt)$_2$]$^{\bullet}$, large longitudinal and lateral slips were noticed with a plane-to-plane distance of 3.63 Å, while the dimerized [Au(EtS-tzdt)$_2$]$^{\bullet}$ complex formed an almost eclipsed overlap with a much shorter plane-to-plane distance, 3.50 Å. The formation of uniform stacks in the case of [Au(HO(CH$_2$)$_2$S-tzdt)$_2$]$^{\bullet}$ complex *vs.* [Au(EtS-tzdt)$_2$]$^{\bullet}$ was attributed to the presence of hydrogen bonding interactions between neighboring stacks. Compared with the hydroxyethyl substituted complex, the *t*Bu groups here induce a slightly larger plane-to-plane distance, without hindering a uniform stacking of the complexes, an advantage for electronic delocalization but also a disadvantage for strong intra-stack interactions necessary for high conductivity. The complex exhibits three types of overlap interactions (I, II, and III) with neighboring molecules within a slab (Fig. 6). The calculated $\beta_{\text{HOMO-HOMO}}$ interaction energies (determined on the molecule with an in-plane orientation of the *t*Bu group) amount to −0.1269, 0.0408, and −0.0019 eV respectively. The interactions along the stacks (type I) are stronger than what was observed for [Au(HOEtS-tzdt)$_2$]$^{\bullet}$, while the two sideway overlap interactions are weaker, indicating a probably more one-dimensional character.

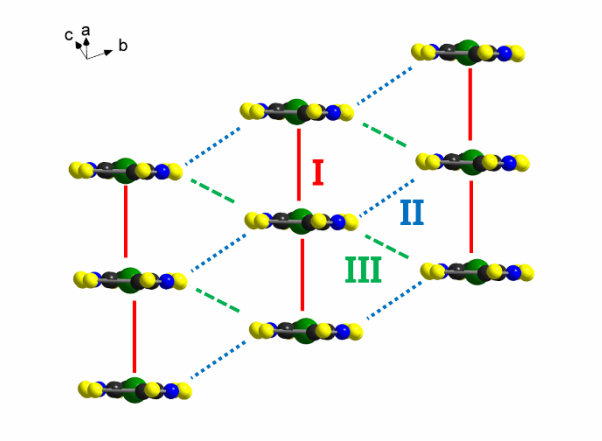

Fig. 6 Side view of the conducting slabs of [Au(*t*BuS-tzdt)$_2$]$^{\bullet}$ with the intermolecular interactions, the *t*Bu groups have been omitted for clarity.

This assumption is confirmed by the calculated band structure for this complex (Fig. 7). It shows indeed a larger band dispersion along the stacks (Γ → X) than in the perpendicular direction. The dispersion itself is rather weak (< 0.5 eV), in accordance with the larger plane-to-plane distance and longitudinal slip mentioned above. Altogether, the structural and electronic properties of this compound suggest a Mott insulating state, i.e. a formally half-filled band system where the band dispersion (W) is too weak to compete with the Hubbard repulsion term *U*. Under such circumstances, the compound is expected to behave as a semiconductor.

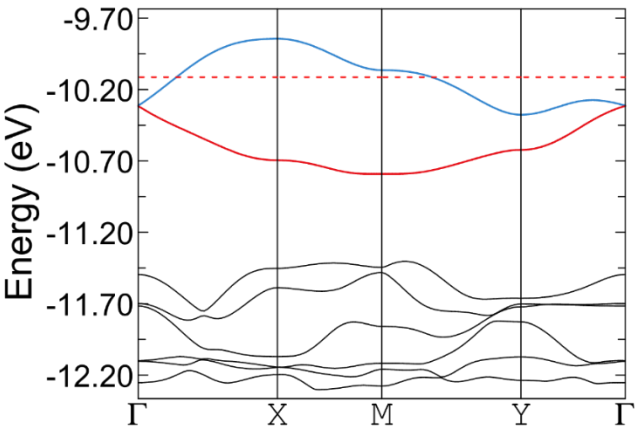

Fig. 7 Calculated band structure for [Au(*t*BuS-tzdt)$_2$]$^{\bullet}$. The HOMO-based band is represented in blue and the HOMO-1 one in red, the dashed red line represents the Fermi level, assuming a metallic filling of the levels. Γ = (0, 0, 0), X = (1/2, 0, 0), M = (1/2, 1/2, 0), Y = (0,1/2, 0) of the Brillouin zone of the monoclinic lattice.

Resistivity measurements confirmed this hypothesis, with a semiconducting behavior observed upon cooling down to 230 K (Fig. 8). The room temperature conductivity was found to be 2.4×10^{-5} S.cm^{-1} with an activation energy of 0.23 eV.

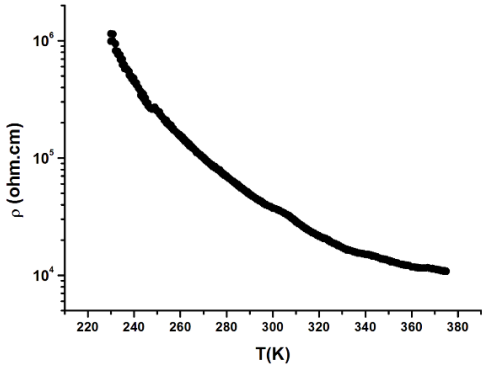

Fig. 8 Temperature dependence of the resistivity of [Au(*t*Bu-S-tzdt)$_2$]$^{\bullet}$.

Conclusions

In this work, we have reported here a new RS-substituted thiazole-based gold complex bearing a bulky *tert*-butyl group [Au(*t*Bu-tzdt)], and explored its electronic and structural properties in the monoanionic and neutral radical state. The solution properties showed an improved stability of the higher oxidation states relative to other complexes of the same family, evidenced by a fully reversible cyclic voltammetry and the observation of the absorption spectra of the monocationic species. Moreover, the bulky *t*Bu group succeeded in preventing dimerization of the neutral species previously seen with the Me and Et analogues, and afforded uniform stacks that are favorable for conducting behavior. However, the weak intra- and inter-stack interactions, along with the disorder of the *t*Bu group resulted in electronic localization and an insulating behavior of the complex. Further studies with different groups are underway to enhance the conducting properties within these series of gold bis(dithiolene) complexes.

Experimental

Reagent and apparatus

Chemicals and materials from commercial sources were used without further purification. All the reactions were performed under an argon atmosphere. Melting points were measured on a Kofler hot-stage apparatus and are uncorrected. Mass spectra were recorded by the Centre Régional de Mesures Physiques de l'Ouest, Rennes. Methanol, acetonitrile and dichloromethane

were dried using Inert pure solvent column device. CVs were carried out on a 10^{-3} M solution of complex in CH_2Cl_2 with NBu_4PF_6 0.1 M. Potentials were measured *versus* Saturated Calomel Electrode (SCE). The spectroelectrochemical setup was performed in CH_2Cl_2 with Bu_4NPF_6 0.2 M using a Pt grid as the working electrode, a Pt wire as the counter electrode and SCE reference electrode. A Shimatzu 3600 spectrophotometer was employed to record the UV-vis-NIR spectra. The proligands **1** was prepared as previously reported.

Synthesis of 5-(*t*butylthio)-1,3-Dithiolo[4,5-*d*]thiazol-2-one 2.

Under inert atmosphere, to a solution of **1** (100 mg, 0.38 mmol) in 5 mL of CH_2Cl_2, iodine crystals (0.38 g, 1.52 mmol) was added. The reaction mixture was set to stirred at 45ºC for 4 hours. The reaction was then quenched with a saturated solution of sodium thiosulfate (100 ml), the product was extracted with CH_2Cl_2 and the organic phase was washed with water and then dried over $MgSO_4$. The solvent was evaporated under vacuum and the crude oil was purified by flash chromatography (eluent: DCM/Petroleum ether; 80:20) giving the compound as a white powder. Yield= 0.036 g, 36%; Rf = 0.73, (SiO_2, CH_2Cl_2); mp = 88 °C; ^{1}H NMR (300 MHz, $CDCl_3$) δ (ppm): 1.48 (s, 9H, CH_3); ^{13}C NMR (75 MHz, $CDCl_3$) δ (ppm): 190.2 (C=O), 162.5 (<u>C</u>=N), 143.6 (C=C), 120.5 (C=C), 51.2 (<u>C</u>-CH_3), 19.9 (CH_3); HRMS (ASAP) calcd for $C_8H_{10}NOS_4^+$: 263.9639, Found : 263.9640; Anal. calcd for $C_8H_9NOS_4$: C, 36.48; H, 3.44; N, 5.32; S, 48.69. Found: C, 36.49; H, 3.29; N, 5.32; S, 48.83.

Synthesis of [PPh$_4$][Au(tBuS-tzdt)$_2$]

Under inert atmosphere, a solution of MeONa (Na: 40 mg, 1.47 mmol) in MeOH (20 mL) was added to the dithiole-2-one **2** (150 mg, 0.57 mmol). After complete dissolution, the solution was stirred for 30 min at room temperature. Then a solution of $KAuCl_4$ (110 mg, 0.29 mmol) in MeOH (5 mL) was added followed 6 hours later by the addition of Ph_4PBr (125 mg, 0.30 mmol). After stirring for 15 h, the formed precipitate was filtered and recrystallized from acetonitrile to afford the monoanionic complex [PPh$_4$][Au(*t*BuS-tzdt)$_2$] as pink crystalline plates. Yield 51% (150 mg). mp = 144°C; ^{1}H NMR (CD_2Cl_2, 300 MHz) δ 7.86 – 7.51 (m, 20H, PPh$_4$), 1.35 (s, 18H, CH_3); ^{13}C NMR (CD_2Cl_2, 75 MHz) δ 161.9 (C=N), 151.9 (C=C), 135.6 (C_{Ar}), 134.4 (C_{Ar}), 130.7 (C_{Ar}), 118.1 (C=C), 116.8 (C_{Ar}), 49.36 (S-<u>C</u>(CH_3)$_3$), 30.9 (S-C(<u>C</u>H$_3$)$_3$); Anal. calcd. for $C_{38}H_{38}AuN_2PS_8$: C, 45.32; H, 3.80; N, 2.78; S, 25.47. Found: C, 44.99; H, 3.94; N, 2.72; S, 25.40.

Electrosynthesis of [Au(tBuS-tzdt)$_2$]$^{\bullet}$

Under inert conditions in a U shaped electrocrystallization cell equipped with Pt electrodes, a supporting electrolyte Me_4NBF_4 (200 mg), and the monoanionic complex (10 mg) were dissolved in a 12 ml of CH_3CN at room temperature. A constant current intensity was adjusted to 0.5 (μA) between the electrodes, and the reaction was left during seven days. Crystals of the neutral complex were collected at the anode.

Band structure calculations

The tight-binding band structure calculations and $\beta_{HOMO/LUMO}$ interaction energies were based upon the effective one-electron Hamiltonian of the extended Hückel method [27], as implemented in the Caesar 2.0 chain of programs [28]. The off-diagonal matrix elements of the Hamiltonian were calculated according to the modified Wolfsberg−Helmholz formula [29]. All valence electrons were explicitly considered in the calculations and the basis set consisted of double-ζ Slater-type orbitals for the metal and chalcogen atoms, and single-ζ Slater-type orbitals for the rest of the atoms.

X-ray diffraction

Suitable crystals of $[PPh_4][Au(tBuS\text{-}tzdt)_2]$and $[Au(tBuS\text{-}tzdt)_2]^{\bullet}$ for X-ray diffraction single crystal experiment were selected and mounted with a cryoloop on the goniometer head of a APEXII Bruker AXS diffractometer, using Mo-Kα radiation (λ = 0.71073 Å, multilayer monochromator). The structures were solved by dual-space algorithm using the *SHELXT* program [30], and the refined with full-matrix least-square methods based on F^2 (*SHELXL*) [31]. All non-hydrogen atoms were refined with anisotropic atomic displacement parameters. H atoms were finally included in their calculated positions. Crystallographic data on X-ray data collection and structure refinements are given in **Table 3**.

Table 3- Crystallographic data.

Compound	$[PPh_4][Au(tBuS\text{-}tzdt)_2]$	$[Au(tBuS\text{-}tzdt)_2]^{\bullet}$
CCDC	2238989	2238990
Formula	$C_{38}H_{38}AuN_2PS_8$	$C_7H_5Au_{0.5}NS_4$
FW ($g\cdot mol^{-1}$)	1007.12	333.87
Crystal system	triclinic	triclinic
Space group	$P\bar{1}$	$P\bar{1}$
a (Å)	11.3191(7)	4.8984(12)
b (Å)	13.5579(9)	6.4182(16)
c (Å)	14.9691(10)	16.954(3)
α	86.600(2)	89.825(6)
β	68.498(2)	86.037(6)
γ	84.332(2)	87.433(7)
V ($Å^3$)	2126.2(2)	531.2(2)
T (K)	296(2)	296(2)
Z	2	2
D_{calc} ($g\cdot cm^{-3}$)	1.859	1.724
μ(mm^{-1})	3.919	2.087
Total refls.	50278	11527
Abs. Corr .	multi-scan	multi-scan
Uniq. refls. (R_{int})	9780(0.0747)	2427(0.0426)
Unique refls. ($I > 2\sigma(I)$)	6659	2327
R_1, wR_2	0.0711, 0.1545	0.0304, 0.0735
R_1, wR_2 (all data)	0.1304, 0.1913	0.0340, 0.0771
GoF	1.156	1.048

Supplementary data

CCDC 2238989 and 2238990 contain X-ray crystallographic files in CIF format for this paper. These data can be obtained free of charge via www.ccdc.cam.ac.uk/data_request/cif, or by emailing data_request@ccdc.cam.ac.uk, or by contacting The Cambridge Crystallographic Data Centre, 12 Union Road, Cambridge CB2 1EZ, UK; fax: + 44 1223 336033.

Acknowledgments

This work was supported by the Université de Rennes 1 (Ph. D. grant for H Hachem)

Contributions

Hadi Hachem realized the experiments and prepared all the figures, Olivier Jeannin performed the X-ray investigations, Dominique Lorcy conceived and designed the complexes, wrote de main manuscript text together with Marc Fourmigué. All the authors reviewed the manuscript.

Corresponding author

Correspondence to Dominique Lorcy: Dominique.lorcy@univ-rennes1.fr

Compliance with ethical standards

Competing interest

The authors declare no competing interests

Conflict of interest

The authors declare that they have no conflict of interest to this work

References

1. Tanaka H, Okano Y, Kobayashi H, Suzuki W, Kobayashi A (2001) Science 291:285-287
2. Garreau de Bonneval B, Moineau-Chane Ching KI, Alary F, Bui TT, Valade L (2010) Coord Chem Rev 254 :1457−1467
3. Naito T (2020) Inorganics 8: 53(1−27)
4. Velho MFG, Silva RAL, Brotas G, Lopes EB, Santos IC, Charas A, Belo D, Almeida M (2020) Dalton Trans 49:13737–13743
5. Cui H, Tsumuraya T, Miyazaki T, Okano Y, Kato R (2014) Eur J Inorg Chem 24:3837–3840
6. Filatre-Furcate A, Bellec N, Jeannin O, Auban-Senzier P, Fourmigué M, Vacher A, Lorcy D (2014) Inorg Chem 53:8681–8690
7. Hadi H, Cui H, Tsumuraya T, Kato R, Jeannin O, Fourmigué M, Lorcy D (2020) J Mater Chem C 8:11581-11592
8. Abhervé A, Mroweh N, Cauchy T, Pop F, Cui H, Kato R, Vanthuyne N, Alemany P, Canadell E, Avarvari N (2021) J. Mater Chem C 9:4119-4140

9. Schultz AJ, Wang HH, Soderholm LC, Sifter TL, Williams JM, Bechgaard K, Whangbo MH (1987) Inorg Chem 26:3757−3761
10. Schiødt NC, Bjørnholm T, Bechgaard K, Neumeier JJ, Allgeier C, Jacobsen CS, Thorup N (1996) Phys Rev B 53:1773−1778
11. Belo D, Alves H, Lopes EB, Duarte MT, GamaV, Henriques RT, Almeida M, Perez-Benítez A, Rovira C, Veciana J (2001) Chem Eur J 7:511−519
12. Andrade MM, Silva RAL, Santos IC, Lopes EB, Rabaça S, Pereira LCJ, Coutinho JT, Telo JP, Rovira C, Almeida M, Belo D (2017) Inorg Chem Front 4:270–280
13. Dautel OJ, Fourmigué M, E. Canadell E, Auban-Senzier P (2002) Adv Funct Mater 12:693−698
14. Higashino T, Jeannin O, Kawamoto T, Lorcy D, Mori T, Fourmigué M (2015) Inorg Chem 54:9908−9913
15. Branzea DG, Pop F, Auban-Senzier P, Clérac R, Alemany P, Canadell E, Avarvari N (2016) J Am Chem Soc 138:6838−6851
16. Tenn N, Bellec N, Jeannin O, Piekara-Sady L, Auban-Senzier P, Íñiguez J, Canadell E, Lorcy D (2009) J Am Chem Soc 131:16961−16967
17. Yzambart G, Bellec N, Nasser G, Jeannin O, Roisnel T, Fourmigué M, Auban-Senzier P, Íñiguez J, Canadell E, Lorcy D (2012) J Am Chem Soc 134:17138−17148
18. Le Gal Y, Roisnel T, Auban-Senzier P, Guizouarn T, Lorcy D (2014) Inorg Chem 53:8755−8761
19. Filatre-Furcate A, Bellec N, Jeannin O, Auban-Senzier P, Fourmigué M, Íñiguez J, Canadell E, Brière B, Ta Phuoc V, Lorcy D (2016) Inorg. Chem. 55:6036-6046
20. Filatre-Furcate A, Roisnel T, Fourmigué M, Jeannin O, Bellec N, Auban-Senzier P, Lorcy D (2017) Chem Eur J 23:16004–16013
21. Le Gal Y, Roisnel T, Auban-Senzier P, Bellec N, Íñiguez J, Canadell E, Lorcy D (2018) J Am Chem Soc 140:69987004
22. Filatre-Furcate A, Auban-Senzier P, Fourmigué M, Roisnel T, Dorcet V, Lorcy D (2015) Dalton Trans 44:15683−15689
23. Hachem H, Bellec N, Fourmigué M, Lorcy D (2020) Dalton Trans 49:6056-6064
24. Hachem H, Jeannin O, Fourmigué M, Barrière F, Lorcy D (2020) CrystEngComm 22:3579-3587
25. Filatre-Furcate A, Roisnel T, Lorcy D (2016) J Organomet Chem 819:182−188
26. Kokatam S, Ray K, Pap J, Bill E, Geiger WE, LeSuer RJ, Rieger PH, Weyhermüller T, Neese F, Wieghardt K (2007) Inorg Chem 46:1100-1111

27. Whangbo MH, Hoffmann R (1978) J Am Chem Soc 100: 6093−6098
28. Ren J, Liang W, Whangbo MH (1998) Crystal and Electronic Structure Analysis Using CAESAR; PrimeColor Software, Inc.: Cary
29. Ammeter JH, Bürgi HB, Thibeault J, Hoffmann R (1978) J Am Chem Soc 100: 3686−3692
30. Sheldrick GM (2015) Acta Cryst A71: 3-5
31. Sheldrick GM (2015) Acta Cryst C71: 3-5